Florencite-(La) with fissiogenic REEs from a natural fission reactor at Bangombé, Gabon

JANUSZ JANECZEK[1] AND RODNEY C. EWING[2]

[1]Faculty of Earth Sciences, University of Silesia, ul. Bedzinska 60, 41-200 Sosnowiec, Poland
[2]Department of Earth and Planetary Sciences, University of New Mexico, Albuquerque, New Mexico 87131, U.S.A.

ABSTRACT

Florencite-(La) (La/Ce = 1.09) with fissiogenic REEs and florencite-(Ce) (La/Ce = 0.62) have been identified in illite from the clay mantle surrounding a natural, 2 Ga fission reactor at Bangombé and in sandstone beneath the reactor zone, respectively. Florencite-(Ce) is apparently unrelated to nuclear processes and occurs with monazite-(Ce), apatite, TiO_2 (probably anatase), zircon, and illite. Grains of florencite-(Ce) contain inclusions of thorite, chalcopyrite, and galena. Florencite-(La) was found 5 cm from the "core" of the reactor and contains inclusions of galena and U-Ti–bearing phases. Secondary uraninite and coffinite have precipitated on some of the florencite grains. The chemical composition of florencite-(La) as determined by electron microprobe analysis is $(La_{0.38}Ce_{0.35}Nd_{0.06}Sm_{0.01}$-$Ca_{0.03}Sr_{0.17})(Al_{2.98}Fe^{3+}_{0.02})(PO_4)[PO_{3.80}(OH)_{0.20}](OH)_6$. Secondary ion mass spectrometry revealed that between 27 and 30% of Nd and 67 and 71% of Sm in florencite-(La) is fissiogenic. The presence of fissiogenic REEs in "florencite" from the reactor zone in Bangombé and their preferential concentration in florencite relative to the bulk sample of clay demonstrate that aluminous phosphates may have played a more significant role in the fixation of fissiogenic REEs released from uraninite after the sustained fission reactions than sorption onto clays.

INTRODUCTION

Spontaneous fission reactions occurred in U deposits of the Franceville Basin in southeastern Gabon at approximately 2 Ga and lasted 10^5–10^6 yr, producing a substantial amount of fission products (Gauthier-Lafaye et al. 1989; Naudet 1991). Sixteen natural fission-reactor zones have been discovered in the U deposit at Oklo since 1972. Two more reactors are known at Okelobondo and Bangombé, some 0.5 and 20 km south of Oklo, respectively. The Bangombé fission reactor, discovered in 1985, is in the upper part of the Proterozoic Franceville sandstone at a depth of 12 m and consists of a 5 cm thick body of a massive U ore (the reactor's "core"), which is overlain by a 30 cm thick clay mantle (Smellie et al. 1993; Bros et al. 1993). U in uraninite from Bangombé is depleted in ^{235}U, with the lowest value of $^{235}U/^{238}U$ = 0.005902, owing to fission reactions (Bros et al. 1993).

Natural nuclear reactors offer a unique opportunity to study the migration of fission products over geologic time; this is relevant to the performance assessment of an underground nuclear waste repository (Naudet 1991). Among fission products, rare earth elements (REEs) are especially well suited for this purpose because their fission yields are high, and they contain strikingly different fissiogenic and natural isotopic compositions (Brookins 1990). Light rare earth elements (LREEs) are good ana-

logs for trivalent transuranic actinides (Krauskopf 1986). Geochemical studies as early as 1975 revealed the redistribution of Nd and heavier REEs in reactor zone 2 at Oklo. The REEs migrated <80 cm (Ruffenach et al. 1975). Curtis et al. (1989) reported that Nd was released from uraninite in reactor zone 9 but was retained within the clay mantle of the reactor zone. Hemond et al. (1992) showed that fissiogenic Nd released from uraninite in reactor zone 10 migrated into the border of the reactor zone and even into the sandstone in areas where calcite-filled fractures were present. They noted that the amounts of released radionuclides and fission products were small in comparison with the quantities produced during fission reactions. Migration of fissiogenic REEs has also been observed in Bangombé. Small amounts of fissiogenic REEs were detected as far as 5.5 m above the reactor core (Bros et al. 1993). None of these observations address the issue of the retention mechanism of released fissiogenic REEs, although the importance of accessory minerals, e.g., zircon, in trapping REEs has been realized (Menet et al. 1992). Recently, Hidaka et al. (1994) showed that apatite inclusions in uraninite at Oklo contain significant amounts of fissiogenic Ce, Nd, and Sm as trace elements in addition to the small amounts of fissiogenic Rb and Ba. We present the results of electron microprobe analyses (EPMA) and secondary ion mass spectrometry (SIMS) of florencite, $(REE)Al_3(PO_4)_2(OH)_6$, from the Bangombé re-
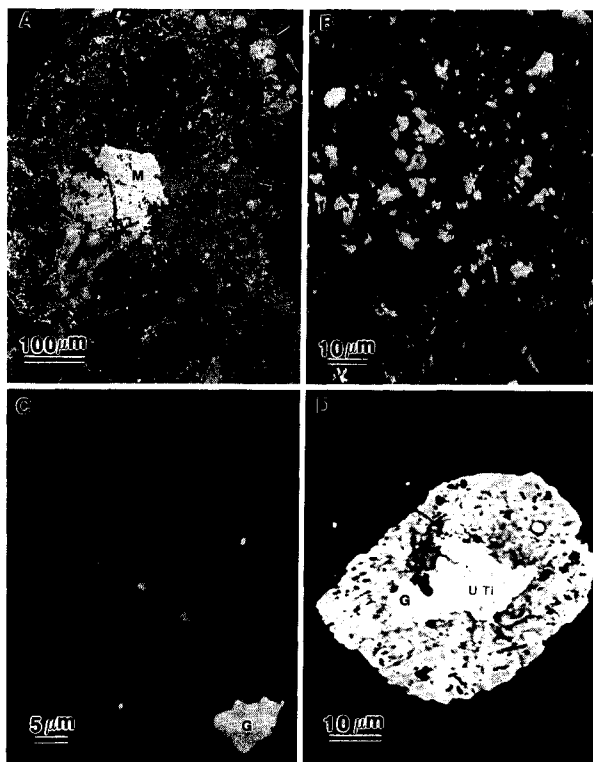
FIGURE 1. (A) Backscattered electron (BSE) image of the matrix in the sandstone from sample BA145-A3 from Bangombé. M = monazite; arrows point to intergrowths of titanium oxide with clay and to grains of florencite-(Ce). Elongated aggregates of florencite also occur in physical contact with monazite (lower left corner). (B) BSE image of florencite-(Ce) with numerous inclusions of thorite and chalcopyrite (both white in the image). (C) BSE image of an aggregate of florencite-(La) crystals in illite (black). G = galena. (D) BSE image of florencite-(La) with core occupied by galena and U and Ti phases.

actor zone, which demonstrate that some of the REEs are the daughters of fission products generated during reactor operation.

"Florencite" is an REE end-member of the crandallite group, which includes aluminous phosphates of Ca (crandallite), Sr (goyazite), Ba (gorceixite), and Pb (plumbogummite), as well as related arsenates (Schwab et al. 1990a). In this paper, we use the term "florencite" in a generic sense, and thus in the remainder of the paper it is not placed in quotes. Florencite occurs in a variety of rock types, including granitic pegmatites, carbonatites, mica schists, hydrothermal deposits, placers, weathered zones [especially in laterites (Lefebvre and Gasparrini 1980; Sawka et al. 1986; Schwab et al. 1989; Slukin et al. 1989)], and shales (Pouliot and Hofmann 1981). In weathered rocks, florencite often occurs as donut-shaped aggregates in cavities after dissolved apatite (Banfield and Eggleton 1989; Braun et al. 1993). Florencite can precipitate at extremely low concentrations of phosphoric acid ($a_{H_3PO_4}$ < 10^{-3}) and at a pH <4 (Schwab et al. 1989).

OCCURRENCE

We found two varieties of florencite in samples from Bangombé: one in sandstone beneath the reactor zone, and the other in illite within the reactor zone.

Florencite outside of the reactor zone occurs in the matrix of the coarse-grained, laminated quartz sandstone (sample BA-145) together with monazite-(Ce), apatite, TiO$_2$ (probably anatase), zircon, and illite (Fig. 1A). Grains of florencite contain numerous inclusions of thorite, chalcopyrite, and galena (Fig. 1B). Though monazite grains are heavily corroded and altered (Fig. 1A), they are not replaced by florencite. In areas where monazite and florencite are in physical contact, the latter is an overgrowth on monazite. Apatite grains are corroded. They have not been seen in physical contact with florencite.

The florencite-bearing sample (5D2B) from the reactor zone was collected from drill hole BAX03 at a depth of 11.75 m, 5 cm above the reactor core (Gauthier-Lafaye, personal communication). The sample consists of illite with veinlets and aggregates of authigenic ferromagnesian chlorite (ripidolite). One of the numerous fractures divides this sample into two portions: one contains florencite, galena, nodules of solid bitumens associated with Ti-, Zr-, and U-rich phases, and U minerals (coffinite and uraninite); the other portion contains abundant pyrite and detrital zircon dispersed within illite. In this latter portion, there is an area of red stain resulting from the oxidation of Fe. Florencite is embedded in the brownish illite and occurs as a train of low-birefringent (0.005), elongated overgrowths of colorless to yellowish rhombohedral crystals up to 110 μm long and 50 μm wide (Fig. 1C). Some florencite grains contain inclusions of galena and U- and Ti-bearing phases (Fig. 1D). Uraninite and coffinite precipitated on florencite and replaced it along fractures (Fig. 2). Precipitation of uraninite on florencite and adjacent illite a few centimeters outside the reactor core suggests that this is a secondary uraninite.

ANALYTICAL METHODS

Samples were analyzed using a JEOL 733 Superprobe operated at an accelerating voltage of 15 kV and a sample current of 20 nA. The beam diameter was ~1 μm. Backscattered electron (BSE) images were obtained at the same operating conditions. Data were reduced (ZAF corrections) using the Oxford GENIE microprobe automation and data-analysis software. P and Al were analyzed by energy-dispersive spectrometry (EDS). Peak profiles for P and Al were generated using data for apatite and corundum, respectively. EDS calibration was performed on an Ni standard. Other elements (Ca, Fe, REEs, S, Si, Th, Ti, U, Y, and Zr) were analyzed in the wavelength-dispersive (WDS) mode. Sr was analyzed by combined EDS and WDS methods because of the overlap of the SrLβ and SiKα peaks. Standards included the minerals andesine for Ca, rutile for Ti, biotite for F, spessartine for Si and Fe, pyrite for S, and thorite for Th, as well as synthetic REEPO$_4$, UO$_2$, and SrMoO$_4$. To distinguish Pb in

uraninite from Pb in galena, S was always analyzed with Pb.

Analyses of isotopic ratios of Nd and Sm were performed by SIMS with the use of CAMECA IMS 4f instrument. Analyses were made by bombardment of the sample with primary O^- ions accelerated through a nominal potential of 10 kV. A primary beam current of 20 nA was focused on the sample over a spot diameter of 25–35 μm. Sputtered secondary ions were energy filtered using a sample offset voltage of 75 V and an energy window of 40 V to effectively eliminate isobaric interferences. Each analysis involved repeated cycles of peak counting on ^{27}Al, ^{143}Nd, ^{145}Nd, ^{146}Nd, ^{147}Sm, and ^{149}Sm, as well as counting on a background position. Peak counting times were varied to achieve an analytical precision of at least 0.2–0.4% for $^{143}Nd/^{146}Nd$ and $^{145}Nd/^{146}Nd$ and 0.8–1.0% for $^{147}Sm/^{149}Sm$. Ratios were corrected for instrumental mass fractionation by comparison with a sample of standard florencite (a variety of stiepelmanite) from a pegmatite in Klein-Spitzkopje, Namibia (Harvard Mineralogical Museum, catalog no. 105/29).

RESULTS AND DISCUSSION

Chemical compositions of florencites and associated minerals

Averaged chemical compositions of florencites and monazite from Bangombé are given in Table 1. The apparent deficiency in P in the electron microprobe analyses of florencite from the sandstone (analyses 5 and 6 in Table 1) reflect the poor quality of the sample surface caused by alteration and inclusions of other minerals. Neither As nor S, which can substitute for P in florencite, were detected. Results of P determinations on the apatite standard, under the same analytical conditions used for the florencite analyses, deviated no more than ±0.2 wt% from the expected value.

To calculate the number of ions in the formula unit of florencite from electron microprobe analysis, florencite's chemical formula must be converted into an anhydrous equivalent. The general chemical formula for phosphates of the crandallite group was recently given by Schwab et al. (1993) as $M^{2+,3+}Al_3(PO_4)_2(OH)_6(H)$, where $M^{2+} = Ca$, Sr, Ba, and Pb, and $M^{3+} = REE$. However, for the purpose of crystal-chemical calculations, we propose the structural formula $(REE^{3+}_{1-x}M^{2+}_x)(Al,Fe)^{3+}(PO_4)[PO_{4-x} \cdot x(OH,F)](OH)_6$, derived by combining the structural formula for M^{2+}-bearing members of the crandallite group, $M^{2+}Al_3(PO_4)(PO_3 \cdot OH)(OH)_6$ (Blount 1974; Radoslovich 1982), with the florencite formula $(REE)Al_3(PO_4)_2(OH)_6$. Although charge balance in the florencite formula is maintained without additional H^+, the replacement of REEs by divalent cations results in a coupled substitution of the type $REE^{3+} = M^{2+} + H^+$. The additional H atom is located on one apical O atom of the PO_4 tetrahedron (Radoslovich 1982); hence, the number of O atoms in this tetrahedron is $O = 4 - OH$. Therefore, the amount of O in the anhydrous formula of florencite, equivalent
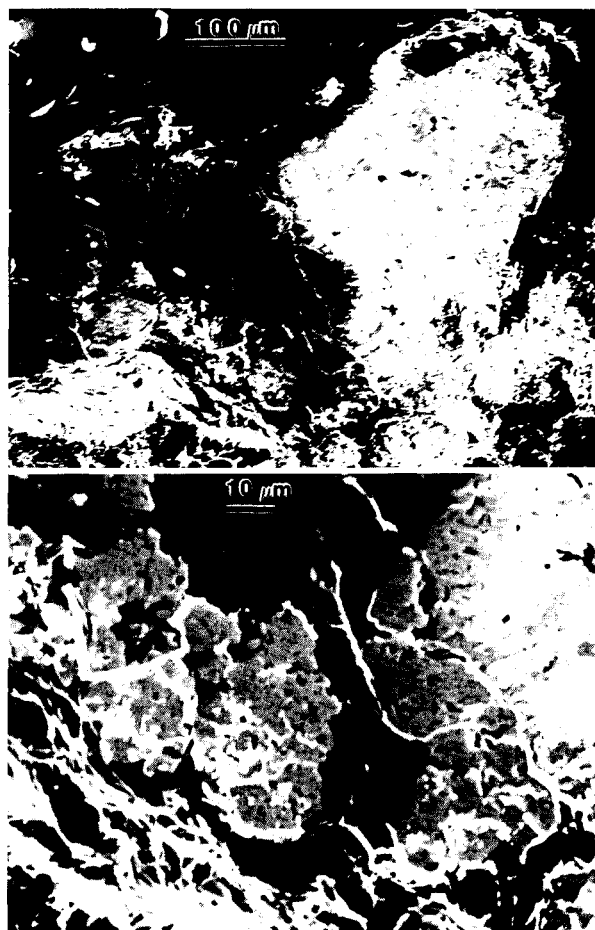

FIGURE 2. Secondary electron image of grains of florencite-(La) in illite (black) partially replaced by uraninite, coffinite, and titanium oxide (white). Lower image shows details of replacement of a florencite grain by U-bearing minerals along fractures. The grain is also decorated with U minerals. Note the feathery appearance of U minerals in clay owing to their precipitation on the (001) planes of illite.

to OH groups, cannot be readily ascertained. To avoid this uncertainty, the number of ions in the florencite formulas in Table 1 were calculated on the basis of six cations in the formula unit $(M^{2+},REE) + (Al,Fe) + P$. The total number of ions of OH^- replacing O^{2-} was calculated by charge balance from $OH = 22 - (\Sigma \text{ cation charges})$, and the amount of O^{2-} replaced by OH^- in PO_4 tetrahedra was calculated from $O = 4 - OH$. The water concentration was then calculated from the amount of OH obtained.

The presence of Sr and Ca in chemical analyses of florencite indicates solid solutions with goyazite and crandallite, respectively (Table 1). Ba and Pb were not detected. Florencite from the reactor zone is enriched in Sr and depleted in Ca relative to the florencite from the sandstone (Table 1). The florencite samples differ in their relative REE abundances. Although Ce is predominant

TABLE 1. Electron microprobe analyses of florencite and monazite from Bangombé

	1	2	3	4	5	6	7
P_2O_5	27.67	27.73	30.75	28.17(30)	26.30(11)	25.80(10)	30.06(29)
SiO_2				b.d.l.	0.07(03)	b.d.l.	0.19(12)
ThO_2				b.d.l.	0.80(71)	0.90(37)	0.06(04)
UO_2				b.d.l.	b.d.l.	0.11(06)	b.d.l.
Al_2O_3	29.81	29.88	33.14	30.12(27)	29.94(09)	30.20(09)	b.d.l.
Fe_2O_3				0.36(08)	1.36(04)	1.71(04)	b.d.l.
Y_2O_3				b.d.l.	b.d.l.	b.d.l.	0.28(05)
La_2O_3		31.83		12.38(54)	8.29(06)	7.42(05)	19.65(36)
Ce_2O_3	31.99			11.31(33)	13.54(06)	14.35(07)	35.28(45)
Nd_2O_3				2.02(23)	3.00(11)	3.03(07)	11.60(39)
Sm_2O_3				0.37(04)	0.58(05)	0.65(05)	2.36(23)
CaO				0.39(07)	0.78(02)	1.03(02)	0.17(08)
SrO			22.45	3.45(44)	1.98(04)	2.02(04)	b.d.l.
H_2O_{calc}	10.53	10.56	13.66	11.13	11.41	11.71	n.d.
Total	100.00	100.00	100.00	99.70	98.05	98.93	99.65
			Number of ions				
			O = 14, Cations = 6				**O = 4**
P	2.00	2.00	2.00	2.00	1.91	1.86	1.00*
Al	3.00	3.00	3.00	2.98	3.03	3.04	
Fe^{3+}				0.02	0.09	0.11	
La		1.00		0.38	0.26	0.23	0.28
Ce	1.00			0.35	0.43	0.45	0.51
Nd				0.06	0.09	0.09	0.16
Sm				0.01	0.02	0.02	0.03
Ca				0.03	0.07	0.09	0.01
Sr			1.00	0.17	0.10	0.10	
O	8.00	8.00	7.00	7.80	7.65	7.50	4.00
OH	6.00	6.00	7.00	6.20	6.35	6.50	

Note: Column numbers refer to the following: 1 = ideal florencite-(Ce), 2 = ideal florencite-(La), 3 = ideal goyazite, 4 = average of fifteen analyses of florencite-(La) from the illite mantle (Bangombé), 5 and 6 = single analyses with the highest analytical total of florencite-(Ce) from sandstone (Bangombé), 7 = monazite-(Ce) from sandstone. Total Fe reported as Fe_2O_3. Values in parentheses refer to the standard deviation of the last two digits; b.d.l. = below detection limit; n.d. = not determined; H_2O_{calc} = calculated from the amount of OH obtained by charge balance.
* Includes 0.01Si.

in the florencite from the sandstone (La/Ce = 0.62), La slightly predominates over Ce in the florencite from the clay (La/Ce = 1.09). REEs other than La, Ce, Nd, and Sm were not detected in either florencite sample, with the detection limits ranging from 0.01 wt% for Y to 0.08 wt% for Tm.

The presence of Th and U in florencite-(Ce) is due mainly to inclusions of thorite (Fig. 1B), and these two elements were not included in the calculation of number of ions in the florencite formula unit. EDS spectra of thorite inclusions showed relatively strong peaks for P but no Al. Therefore, P may substitute for Si in the thorite structure. The low content of Th in monazite (Table 1) is unusual because monazite commonly contains significant amounts of Th and U, occasionally over 15 wt% UO_2 and 14 wt% ThO_2 (Boatner and Sales 1988). The absence of Th in monazite could have been caused by a preferential leaching of Th during alteration of the monazite. Released Th was precipitated as thorite.

Because of the small grain size and intergrowths with other phases, it was extremely difficult to obtain reliable microprobe analyses of the U-bearing phases that precipitated on the reactor-zone florencite (Fig. 2). The average of three analyses of a single uraninite grain <10 μm in size is (in weight percent) UO_2 85.13(17), SiO_2 1.63(12), PbO 4.76(31), FeO 0.31(01), Al_2O_3 0.28(02), and P_2O_5 0.32(01). Al and P are from the associated florencite. Silica may be related to minor coffinite. One analysis of the

U-rich material gave SiO_2 and UO_2 contents close to the coffinite stoichiometry ($USiO_4 \cdot nH_2O$). Otherwise, the SiO_2 contents varied from 1.4 to 8.8 wt%, suggesting that the SiO_2 could be, in part, associated with different amounts of coffinite replacing uraninite. All analyzed U-rich material contained significant Ti (up to 2 wt% TiO_2) with the exception of the analyzed uraninite grain.

Isotopic ratios

Values of Nd and Sm isotopic ratios ($^{143}Nd/^{146}Nd$, $^{145}Nd/^{146}Nd$, $^{149}Sm/^{147}Sm$) obtained by SIMS in florencite-(La) are given in Table 2 and compared with a standard florencite-(Ce) from a pegmatite in Namibia, a sample of clay in which florencite-(La) occurs, a sample of U ore from the core of the reactor zone at Bangombé (Bros et al. 1993), and the fission REE-bearing apatite from reactor zone 10 at Oklo (Hidaka et al. 1994). Values of Nd and Sm isotopic ratios for those samples normalized to the normal isotopic ratios are shown in Figure 3. The isotopic ratios shown in Table 2 and Figure 3 for florencite-(La) from the Bangombé nuclear reactor are distinctly different from the isotopic ratios for "normal" florencite. Observed isotopic ratios (R_o) include ratios of the abundances of natural isotopes (R_n) and ratios of the abundances of fissiogenic isotopes (R_f); therefore,

$$R_o = xR_n + yR_f \qquad (1)$$

where x and y are the proportions of the natural and

TABLE 2. Isotopic ratios of Nd and Sm in florencite

Sample	$^{143}Nd/^{146}Nd$	$^{145}Nd/^{146}Nd$	$^{149}Sm/^{147}Sm$
Florencite (A) 5D2	0.9585(17)	0.6670(13)	0.3284(25)
Florencite (B) 5D2	0.9536(33)	0.6608(24)	0.2938(29)
Florencite, STD	0.7031(12)	0.4803(12)	0.9180(34)
Bulk sample 5D2*	0.8725	0.6007	0.4365
Bulk sample 5D1*	1.4695	1.0240	0.1012
Apatite SF29-8612**	1.6354	1.2047	0.0065
Natural abundance	0.7034	0.4803	0.9184

Note: Two grains (A and B) of florencite from illite in sample 5D2 from the Bangombé reactor zone; florencite from pegmatite in Namibia (STD); bulk samples 5D2 (clay mantle) and 5D1 (core of the Bangombé reactor zone), and apatite from reactor zone 10 at Oklo. Mean deviations are given in parentheses.
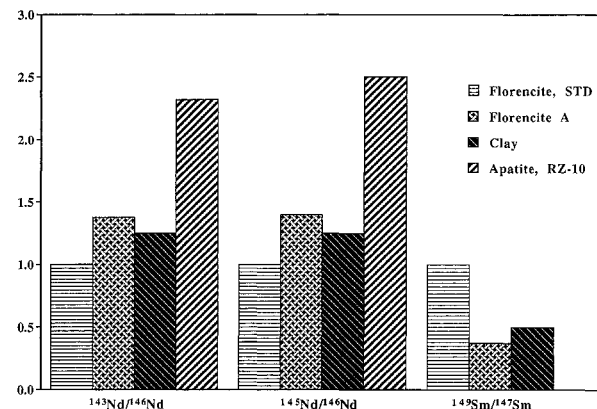* Ratios calculated on the basis of data in Bros et al. (1993).
** Ratios calculated on the basis of data in Hidaka et al. (1994).

FIGURE 3. Bar chart of isotopic ratios in florencite with normal isotopic abundances, florencite-(La) from Bangombé, illitic clay hosting the florencite-(La), and apatite from reactor zone 10 at Oklo, normalized to the normal isotopic ratios of Nd and Sm.

fissiogenic isotopes, respectively, to the total. The proportion of the fissiogenic isotope to the total can be calculated from the equation $R_o = (1 - y)R_n + yR_f$, which is rearranged to give

$$y = (R_o - R_n)/(R_f - R_n). \qquad (2)$$

We were not able to measure isotopes with a low fission-product yield, i.e., ^{142}Nd and ^{144}Sm, which are commonly used as reference (natural) isotopes in the calculation of the ratio of natural to fissiogenic Nd and Sm (Hidaka et al. 1988; Hemond et al. 1992). Thus, in these calculations we used ratios of the abundances of fissiogenic isotopes measured in apatite from the core of reactor zone 10 at Oklo with 93 and 96% fissiogenic Nd and Sm, respectively (Hidaka et al. 1994). Therefore, values of y obtained from Equation 2 were normalized to 100% by dividing y by 0.93 for Nd and by 0.96 for Sm. On the basis of these calculations, between 27 and 30% of the Nd and 67 and 71% of the Sm in the florencite-(La) is fissiogenic. Assuming that there was no production of fissiogenic ^{149}Sm, i.e., $R_f = 0$, because of a small neutron-capture cross section of ^{149}Sm, the proportion of natural isotope to the total calculated from Equation 1 is $x = R_o/R_n = 0.36$; thus, 64% of the Sm is fissiogenic. These abundances are lower than the abundances of fissiogenic REEs in apatite from the core of reactor zone 10 (Hidaka et al. 1994). However, although the highest concentrations of fissiogenic Nd and Sm in the apatite are 501 and 60 ppm, respectively, the highest concentrations of fissiogenic Nd and Sm observed in florencite are 3.1 and 0.2 wt%, respectively. The abundances of fissiogenic Nd and Sm in florencite are higher than the abundances of fissiogenic Nd (19.9%) and Sm (52.6%) observed by Bros et al. (1993) in the bulk sample of the clay mantle (Table 2; Fig. 3). The enrichment in fissiogenic Nd and Sm in florencite relative to the other components of the clay mantle suggests that LREE nuclides were preferentially incorporated into the florencite structure during the influx of fissiogenic LREEs, which were released from uraninite. The crystal-chemical properties of crandallite, especially Sr-rich crandallite, makes it an efficient trap for LREEs (Schwab et al. 1990b). The crystallization of LREE alu-

minous phosphates was also favored by the peraluminous composition of the clay mantle. Because of these two factors, florencite may be a common but so far overlooked accessory mineral in the clay mantles of all the reactors.

Traces of ^{135}Ba and ^{137}Ba were detected in florencite-(La) (counts from ^{135}Ba and ^{137}Ba were 2.0×10^2 and 3.5×10^2 cps, respectively; in comparison, the count for ^{27}Al is 2.92×10^6 cps). Their progenitors were Cs isotopes, ^{135}Cs and ^{137}Cs. Finding phases enriched in radiogenic Ba is crucial to understanding the behavior of ^{137}Cs in natural reactors (Hidaka et al. 1992). Traces of fissiogenic Ba (up to 3 ppm) have been observed in apatite from the core of reactor zone 10 (Hidaka et al. 1994).

Although we could not determine the isotopic composition of LREEs in florencite-(Ce) from the sandstone, their occurrence in the sandstone matrix together with apparently detrital and altered monazite-(Ce) and apatite suggests that the origin of florencite-(Ce) is different from that of the florencite-(La) in the reactor zone. Alteration of monazite-(Ce) and apatite was probably a source of P and REEs for the formation of florencite-(Ce) in the sandstone.

Timing of the florencite-(La) formation

An important question is that of the timing of REE mobilization in the reactor zone. Precipitation of a secondary uraninite on florencite (Fig. 2) suggests that the florencite is older than the uraninite. There were at least two stages of U mobilization in the natural reactors. The first was related to the partial dissolution of uraninite caused by the formation of a clay halo around the uraninite (Janeczek and Ewing 1995) during or shortly after the sustained nuclear reactions of 2 Ga (Gauthier-Lafaye et al. 1989). The second stage of U migration from the cores of the reactors was related to the hydrothermal alteration of uraninite caused by the igneous activity in the Franceville Basin at 750–720 Ma (Nagy et al. 1991; Hemond et al. 1992; Holliger 1992). Also associated with

this thermal event was total, or almost total, Pb loss from uraninite in most of the reactor zones (Janeczek and Ewing 1995). The bulk Pb concentration in the uraninite precipitated on florencite (4.8 wt% PbO) is within the range of Pb concentrations in uraninite from all the reactor zones affected by the second event (Janeczek and Ewing 1995). Therefore, precipitation of the secondary uraninite on florencite places an upper limit on the time of florencite crystallization. A few florencite grains contain inclusions of U phases and galena (Fig. 2). Unfortunately, neither the age of the uraninite nor that of the galena is known. Because of the multistage alteration of uraninite, galenas of different ages are expected to occur in the natural reactors. Galena with a $^{207}Pb/^{206}Pb$ age of 1788 ± 4 Ma has been observed in reactor zone 9 at Oklo (Nagy et al. 1991). All Pb in that galena is radiogenic; therefore, the galena is only 200 m.y. old. Recent geochemical data suggest that REEs were stable relative to U during the second stage of uraninite alteration at Bangombé (Bros et al. 1993), and, therefore, REEs were released mainly during or shortly after criticality. However, earlier geochemical studies showed that no significant migration of REEs occurred during the nuclear reactions at the Oklo deposit (Loubet and Allegre 1977). Textural observations of the paragenetic relations between florencite and illite are inconclusive. Illite at the contact with florencite is deformed as if pushed apart by crystallizing grains of florencite, which may indicate that the florencite, is younger than illite. Clearly, more observations are needed to address the problem of the age of the fissiogenic REE-bearing florencite.

Florencite is not the only mineral known to have incorporated fissiogenic elements as major constituents. Ru-, Pb-, Rh-, and Pd-rich sulf-arsenides and arsenides have been found adjacent to uraninite in the cores of reactor zones 10 and 13 (Holliger 1992; Hidaka et al. 1994; Janeczek and Ewing 1995). Ru in these minerals contains up to 46.6% ^{99}Ru, a daughter of ^{99}Tc (Holliger 1992). Also, molybdenite observed at the interface between uraninite and clay in a sample from reactor zone 10 may contain fissiogenic Mo (Janeczek and Ewing 1995). However, although Ru-rich particles and molybdenite occur in the immediate vicinity of uraninite, fissiogenic LREE-bearing florencite-(La) occurs outside the reactor core.

CONCLUSIONS

The occurrence of florencite, which contains fissiogenic REEs, in the clay mantle surrounding the core of the natural fission reactor at Bangombé provides mineralogic evidence for one of the possible mechanisms of fixation of REEs released from uraninite after the sustained fission reactions. Preferential concentration of fissiogenic Nd and Sm in the florencite relative to the bulk sample of the clay demonstrates that aluminous phosphates may have played a more significant role in the fixation of migrating REEs than sorption onto clays.

REFERENCES CITED

Banfield, J.F., and Eggleton, R.A. (1989) Apatite replacement and rare earth mobilization, fractionation, and fixation during weathering. Clays and Clay Minerals, 37, 113–127.

Blount, A.M. (1974) The crystal structure of crandallite. American Mineralogist, 59, 41–47.

Boatner, L.A., and Sales, B.C. (1988) Monazite. In W. Lutze and R.C. Ewing, Eds., Radioactive waste forms for the future, p. 495–564. North-Holland, Amsterdam.

Braun, J.-J., Pagel, M., Herbillon, A., and Rosin, Ch. (1993) Mobilization and redistribution of REEs and thorium in a syenitic lateritic profile: A mass balance study. Geochimica et Cosmochimica Acta, 57, 4419–4434.

Brookins, D.G. (1990) Radionuclide behavior at the Oklo nuclear reactor, Gabon. Waste Management, 10, 285–296.

Bros, R., Gauthier-Lafaye, F., Larque, P., and Stille, P. (1993) Mineralogy and isotope geochemistry of Bangombe reaction zone: Migration of U, Th and fission products. SKB-CNRS "Oklo-Analogues Naturels" Report.

Curtis, D., Benjamin, T., Gancarz, A., Loss, R., Rosman, K., DeLaeter, J., Delmore, J.E., and Maeck, W. (1989) Fission product retention in the Oklo natural fission reactors. Applied Geochemistry, 4, 49–62.

Gauthier-Lafaye, F., Weber, F., and Ohmoto, H. (1989) Natural fission reactors of Oklo. Economic Geology, 84, 2286–2295.

Hemond, C., Menet, C., and Menager, M.T. (1992) U and Nd isotopes from the new Oklo reactor 10 (Gabon): Evidence for radioelements migration. Materials Research Society Symposium Proceedings, 257, 489–496.

Hidaka, H., Masuda, A., Fuji, I., and Shimizu, H. (1988) Abundance of fissiogenic and pre-reactor natural rare-earth elements in a uranium ore sample from Oklo. Geochemical Journal, 22, 47–54.

Hidaka, H., Konishi, T., and Masuda, A. (1992) Reconstruction of cumulative fission yield and geochemical behavior of fissiogenic nuclides in the Oklo natural reactors. Geochemical Journal, 26, 227–239.

Hidaka, H., Takahashi, K., and Holliger, Ph. (1994) Migration of fission products into micro-minerals of the Oklo natural reactors. Radiochimica Acta, 66/67, 463–468.

Holliger, Ph. (1992) The new Oklo reaction zones: U-Pb dating and in situ characterization of fission products by ion analysis. CEA Report 01/92. Centre d'Etudes Nucléaires de Grenoble (in French).

Janeczek, J., and Ewing, R.C. (1995) Mechanisms of lead release from uraninite in the natural fission reactors in Gabon. Geochimica et Cosmochimica Acta, 59, 1917–1931.

Krauskopf, K.B. (1986) Thorium and rare-earth metals as analogs for actinide elements. Chemical Geology, 55, 323–335.

Lefebvre, J.-J., and Gasparrini, C. (1980) Florencite, an occurrence in the Zairian copperbelt. Canadian Mineralogist, 18, 301–311.

Loubet, M., and Allegre, C.J. (1977) Behavior of the rare earth elements

in the Oklo natural reactor. Geochimica et Cosmochimica Acta, 41, 1539–1548.

Menet, C., Ménager, M.-T., and Petit, J.-C. (1992) Migration of radio-elements around the new nuclear reactors at Oklo: Analogies with a high-level waste repository. Radiochimica Acta, 58/59, 395–400.

Nagy, B., Gauthier-Lafaye, F., Holliger, P., David, D.W., Mossman, D.J., Leventhal, J.S., Rigali, M.J., and Parnell, J. (1991) Organic matter and containment of uranium and fissiogenic isotopes at the Oklo natural reactors. Nature, 354, 472–475.

Naudet, R. (1991) Oklo: Des Réacteurs nucléaires fossiles, 685 p. étude physique, Eyrolles, Paris.

Pouliot, G., and Hofmann, H.J. (1981) Florencite: A first occurrence in Canada. Canadian Mineralogist, 19, 535–540.

Radoslovich, E.W. (1982) Refinement of gorceixite structure in Cm. Neues Jahrbuch für Mineralogie Monatshefte, 10, 446–464.

Ruffenach, J.-C., Menes, J., Lucas, M., Hagemann, R., and Nief, G. (1975) Detail isotopic analysis of fission products and determination of the principal parameters of nuclear reactions. IAEA-SM-204, International Atomic Energy Agency, Paris, 371–384 (in French).

Sawka, W.N., Banfield, J.F., and Chappell, B. (1986) A weathering-related origin of widespread monazite in S-type granites. Geochimica et Cosmochimica Acta, 50, 171–175.

Schwab, R.G., Herold, H., Da Costa, M.L., and De Oliveira, N.P. (1989) The formation of aluminous phosphates through lateritic weathering of rocks. In Weathering: Its products and deposits, vol. II: Products-deposits-geotechnics, p. 369–386. Theophrastus, Athens.

Schwab, R.G., Herold, H., Götz, Ch., and De Oliveira, N.P. (1990a) Compounds of the crandallite type: Synthesis and properties of pure goyazite, gorceixite and plumbogummite. Neues Jahrbuch für Mineralogie Monatshefte, 3, 13–126.

——— (1990b) Compounds of the crandallite type: Synthesis and properties of pure rare earth element-phosphates. Neues Jahrbuch für Mineralogie Monatshefte, 6, 241–254.

Schwab, R.G., Götz, Ch., Herold, H., and De Oliveira, N.P. (1993) Compounds of the crandallite type: Thermodynamic properties of Ca-, Sr-, Ba-, La-, Ce- to Gd-phosphates and-arsenates. Neues Jahrbuch für Mineralogie Monatshefte, 12, 551–568.

Slukin, A.D., Arapova, G.A., Zvezdinskaya, L.V., Tsvetkova, M.V., and Lapin, A.V. (1989) Mineralogy and geochemistry of laterized carbonatites of the USSR. In Weathering; Its products and deposits, vol. II: Products-deposits-geotechnics, p. 171–189. Theophrastus, Athens.

Smellie, J.A.T., Winberg, A., and Karlsson, F. (1993) Swedish activities in the Oklo natural analogue project. In H. von Maravic, Ed., Proceedings of the 2nd joint CEC-CEA meeting, p. 137–148. Luxembourg, Brussels 1992.